Journal of Sol-Gel Science and Technology
https://doi.org/10.1007/s10971-024-06510-w

ORIGINAL PAPER

Hybrid Polyvinyl Alcohol-Silica Antibacterial Nanofiber Fabricated by Combined Sol-Gel and Electrospinning Techniques

Khadija El Kalaaoui[1,2] · Aicha Boukhriss[3] · Oumaima Bili[1,2] · Mohamed Ait Chaoui[1] · Sanaa Majid[4] · Mohamed El Hajaji[2] · Said Gmouh[1]

Received: 21 May 2024 / Accepted: 1 August 2024

Abstract

Organic-inorganic hybrids are valuable due to their combined properties. This study fabricated polymer-silica hybrid nanofibers with antibacterial properties using silica and polyvinyl alcohol (PVA) through sol-gel and electrospinning methods. The nanofibers, incorporating chloropropyltriethoxysilane (CPTS) and Benzalkonium chloride (BAC), were analyzed for their morphology, chemical composition, mechanical properties, thermal properties, and antibacterial activity. Optimal characteristics in fibrous structure, mechanical strength, and antibacterial efficiency were achieved with a blended 8% wt PVA. Sample H, containing 1% BAC, showed significant bacterial growth inhibition (20 mm for Staphylococcus aureus and 9.2 mm for Escherichia coli), along with enhanced thermal stability (260.41 °C) and tensile strength (12.4 MPa). This study demonstrates the potential of electrospinning in creating advanced hybrid nanofibers with diverse applications in the medical field.

Graphical Abstract

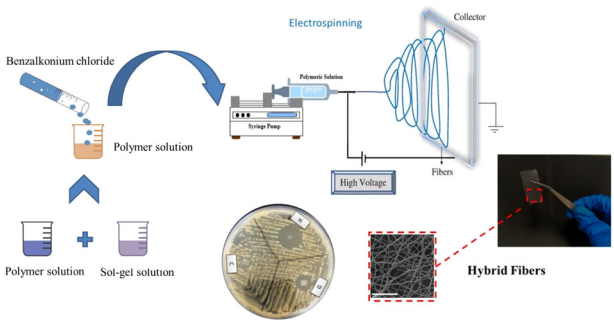

Keywords Electrospinning · Hybrid · Nanofiber · Sol-gel · Antibacterial · Polyvinyl alcohol · Silica

Highlights

- Fabrication of polymer-silica hybrid nanofibers with outstanding antibacterial properties.
- Utilization of sol-gel and electrospinning methods in the fabrication process.

✉ Said Gmouh
s.gmouh1@gmail.com

[1] Laboratory of Engineering and Materials (LIMAT), Faculty of Sciences Ben M'Sik, Hassan II University of Casablanca, Casablanca, Morocco

[2] The Multi laboratory LC2A, N°182, Zone Industrielle, Mohammedia, Morocco

[3] Cluster Valbiom, IMM RIHAB 6EME ETAGE APPT21, Oujda 60000, Morocco

[4] Laboratory of Materials Engineering for the Environment and Valorization, Faculty of Sciences Aïn Chock, Hassan II University of Casablanca, Casablanca, Morocco

Published online: 11 August 2024

- Comprehensive analysis of nanofiber morphology, chemical composition, mechanical and thermal properties, and antibacterial activity.
- Highlighting the potential of electrospinning for creating advanced hybrid nanofibers with versatile applications.

1 Introduction

Hybrid nanofibers have attracted significant attention due to their unique characteristics, encompassing magnetic, optoelectrical, and biological properties that hold substantial importance in fields like optics, energy generation, environmental applications, medicine, and biotechnology [1, 2]. Multiple methods exist for creating hybrid nanofiber-based structures, enabling the production of both two-dimensional (2D) and three-dimensional (3D) nanofibers, which is highly significant [3].

Electrospinning technology has gained increasing interest as a means to produce hybrid fibers.

Recent advancements have expanded its capabilities from the single-fluid blending process [4, 5] to more sophisticated techniques like bi-fluid coaxial electrospinning [6], side-by-side electrospinning [7], and multiple-fluid triaxial electrospinning [8]. Additionally, innovative methods such as Janus electrospinning [9, 10] and their combinations [11, 12] are being explored to produce new types of nanofibers. Recent research highlights the potential of such antibacterial hybrid nanofibers in various applications, including wound dressings and tissue engineering, demonstrating their ability to provide enhanced antibacterial properties and biocompatibility. These advancements demonstrate that electrospinning can be integrated with various traditional chemical and physical methods, significantly broadening the capability of preparing novel nanofibers [13–16].

Electrospun nanofibers possess exceptional qualities, including high surface-to-volume ratios, substantial porosity, cost-effectiveness, ease of fabrication, surface customization, and adjustable fiber morphology, rendering them appealing for diverse applications [17–19]. Hybrid nanofibers can be fabricated from a wide range of natural and synthetic polymers [20–22]. Biopolymers, being non-toxic and displaying superior biocompatibility and biodegradability relative to synthetic ones, may additionally exhibit unique biological properties like antibacterial and antifungal effects. However, biopolymers generally exhibit lower mechanical properties than synthetic polymers [23, 24].

Moreover, the sol-gel technique presents the opportunity to synthesize inorganic materials or a blend of inorganic and organic materials at low temperatures via solution gelation. The initial phase in any sol-gel process entails selecting a suitable precursor for the desired end materials. This precursor should be capable of undergoing hydrolysis reactions and assisting in forming colloidal particles or polymeric gels [25, 26]. A variety of precursors, such as tetraethoxysilane (TEOS), tetramethoxysilane (TMOS), Chloropropyltriethoxysilane (CPTS), tetraethoxysilane, aluminum isopropoxide, others, can be employed [27]. Once hydrolyzed, it reacts with other functional groups, leading to the development of a hybrid network [28]. Various parameters, including the choice of precursor, can influence the sol-gel technique's outcomes.

In this context, Yanilmaz et al. [29] have fabricated silica/polyacrylonitrile (SiO2/PAN) hybrid nanofiber membranes using sol-gel and electrospinning techniques. These membranes were evaluated for their electrochemical performance as potential separators in lithium-ion batteries, aiming to create separators with improved electrochemical properties and thermal stability compared to traditional microporous polyolefin membranes. The authors successfully incorporated SiO2 nanoparticles into the membranes through the sol-gel method, achieving a content of up to 27 wt%. As a result, the SiO2/PAN hybrid nanofiber membranes exhibited superior electrochemical performance and excellent thermal stability due to their high SiO2 content and significant porosity. In a similar study, Jafari et al. [30] developed carbon-silica hybrid fibers for a coating in solid-phase microextraction. This synthesis was achieved through a sol-gel and electrospinning process, utilizing PAN (polyacrylonitrile) and TEOS (tetraethyl orthosilicate) as the carbon and silica precursors, respectively. These porous hybrid nanofibers were fabricated in a single step through a straightforward thermal treatment. Incorporating TEOS into the PAN solution led to an augmentation of the specific surface area, thereby improving the extraction performance of the hybrid nanofibers.

These advancements demonstrate that electrospinning can be integrated with various traditional chemical and physical methods, significantly broadening the capability of preparing novel nanofibers.

Therefore, this study aims to combine the electrospinning and sol-gel methods to develop a hybrid nanofiber. Polyvinyl alcohol (PVA) was chosen because it is a biocompatible and biodegradable polymer. It has been widely used in various applications due to its excellent properties, such as low toxicity, biodegradability, and thermal stability [31]. However, PVA alone has some limitations, such as poor mechanical properties. To overcome this limitation, the silica precursor, Chloropropyltriethoxysilane (CPTS), was selected due to its excellent thermal stability, mechanical strength, and chemical resistance. Additionally, TEOS was used in this study solely for comparative purposes to highlight the effectiveness of CPTS in forming more robust electrospun films than TEOS.

Therefore, combining PVA with silica to create a hybrid material can improve properties and new potential applications. Initially, the optimization of the fiber was prioritized to establish the correct formulation for desirable mechanical and structural characteristics. Subsequently, an antibacterial agent, Benzalkonium chloride (BAC), was introduced into the nanofibrous structures to enhance the functionality of these hybrid nanofibers. BAC, an organic cationic surfactant with quaternary ammonium groups, was chosen for its antibacterial activity [32]. It is widely used in various applications in antisepsis, disinfection, or preservation in industrial, medical, and domestic fields, due to its efficacy, low toxicity, and broad range of target organisms [33, 34]. This study specifically focuses on developing an antibacterial hybrid nanofiber of silica and PVA fabricated through the sol-gel and electrospinning processes.

2 Materials and Methods

2.1 Materials

Chloropropyltriethoxysilane (CPTS, Mw = 240.79 g/mol, 98%), Tetraethyl orthosilicate (TEOS, Mw = 208.33 g/mol, 99%) Hydrochloric acid (HCl, 37%), Dimethylformamide (DMF, 99%), Benzalkonium chloride (BAC, ≥ 50%), and Polyvinyl alcohol (PVA) (Mw 146,000–186,000) were purchased from Sigma Aldrich. All reagents were used as received.

2.2 Preparation of Hybrid Nanofiber Solution

The hybrid nanofibers were fabricated using a sol-gel method to create a silica precursor solution, which was subsequently electrospun with PVA. The silica precursor solution was prepared: CPTS, DMF, and HCl were mixed in a molar ratio of 1/30/0.04 (CPTS/DMF/HCl) [19]. Specifically, 2.4 ml of CPTS was added to 24 ml of DMF and stirred for 10 min. Then, 4 ml of HCl (0.1 mol/l) was added. This solution was transferred to a round-bottom flask, attached to a reflux condenser, and allowed to react at 70 °C for 3 h until a homogeneous solution was formed. PVA was dissolved in 10 ml of distilled water in varying masses (0.5, 0.8, 1, 1.5, and 2 g) to achieve concentrations of 5, 8, 10, 15, and 20 wt% (m/v) (see Table 1). These solutions were stirred with a magnetic stirrer at 90 °C for 4 h. The silica precursor solution was then combined with the PVA solution in a volume ratio 1:1, and the mixture was stirred for 1 h until a homogeneous solution was achieved. Similarly, a TEOS precursor solution was prepared using the same molar ratios of TEOS, DMF, and HCl and processed under the same conditions. This setup was used to compare the effectiveness of TEOS with CPTS in forming electrospun films. The best polymer concentration and formulation that yielded the highest quality fibers with CPTS were also used with TEOS to compare their fiber-forming capabilities directly, thus providing a comprehensive evaluation of both precursors' performance in creating robust electrospun films (see Table 1).

Table 1 Hybrid nanofiber composition

Sample	molar ratio of the sol-gel solution	PVA concentration wt % (m/v)	BAC percent (%)
A	0	8	–
B	CPTS/DMF/HCl 1/30/0,04	5	–
C		8	–
D		10	–
E		15	–
F		20	–
G		8	0.1
H		8	1
T	TEOS/DMF/HCl 1/30/0,04	8	–

2.3 Electrospinning

The electrospinning solutions prepared as described in Section "Preparation of Hybrid Nanofiber Solution" were transferred into a 10 ml syringe. Electrospinning was then performed using a Nanospinner (Inovenso NS + NanoSpinner Plus Electrospinning Unit), with an applied voltage ranging from 30 kV. The flow rate was set between 1 mL/h and the distance between the collector and the nozzle was fixed at 10 cm. The hybrid nanofibers produced were collected on wax paper.

2.4 Preparation of Antibacterial Hybrid Nanofiber

Antibacterial hybrid nanofibers were fabricated using the optimal fiber-forming electrospun solution prepared in Section "Preparation of Hybrid Nanofiber Solution". To this solution, BAC was added as an antibacterial agent in concentrations of 0.1 wt% and 1 wt% (Table 1). The mixture was stirred for 1 h until a homogeneous solution was obtained. After this preparation, the electrospinning process for these solutions was carried out as detailed in Section "Electrospinning".

2.5 Characterization Techniques

2.5.1 Morphology Characterization

The samples' morphology was evaluated using a Phenom ProX scanning electron microscope (SEM) with an energy-dispersive X-ray detector (EDX). The acceleration voltage was set at 15 kV to obtain high-resolution images (without any treatment). Images of the fibers were taken to measure

the fiber diameter and 100 fiber diameters were measured for each sample. X-ray spectroscopy (EDX) system with a Backscattered Electron Detector (BSD) was used to obtain qualitative chemical element analysis.

2.5.2 Chemical Composition

Fourier studied the chemical composition and the characteristics of the produced hybrid nanofibers transform infrared spectroscopy FTIR to record the spectrum with a PerkinElmer 400 spectrometer operating in the 400 to 4000 cm-1 range.

2.5.3 Mechanical Properties

The tensile properties of the samples were evaluated using a testing machine with a load cell of 250 N according to the ASTM D882-18 standard. Rectangular strip samples were prepared with dimensions of 50 × 10 mm. Tensile stress-strain curves were obtained when the samples were stretched at a 5 mm/min speed. The tensile strength, elongation at break, and Young's modulus were determined from the stress-strain curves, with average values calculated based on three specimens from each group.

2.5.4 Thermal Stability

The thermal stability of samples was analyzed by differential scanning calorimetry (DSC, Shimadzu-Japan). A 10–12 mg sample was sealed in an aluminum pan and heated between room temperature and 300 °C at a heating rate of 10 °C per minute in the presence of nitrogen as an inert carrier gas.

2.5.5 Antibacterial Activity

To evaluate the antibacterial properties of the samples, Staphylococcus aureus (S. aureus) (ATCC 25923) and Escherichia coli (E.c oli) (ATCC 8739) were used as test organisms in the zone of inhibition test. Bacterial solutions with a concentration of (106 CFU/mL) were dispensed onto an agar plate. Pieces of 0.5 cm × 0.5 cm were placed on the surface of the plate. The zone of inhibition was measured after 24-h incubation at 37 °C.

3 Results and Discussion

3.1 Antibacterial Hybrid Nanofiber Optimization

3.1.1 Morphology of Hybrid Nanofiber

The morphology of nanofibers, as revealed by images recorded by SEM (Fig. 1), demonstrates several exciting trends based on the different percentages of polymer in the electrospinning solutions. PVA nanofiber (sample A) gave rise to fibers of standard diameter (0, 83 µm), setting a reference for the size of fibers produced under these conditions. However, sample B could not generate fibers, suggesting that the polymer concentration at this level is insufficient to induce the fiber formation process. Sample C produced fine fibers with a diameter of 119 nm, indicating that this concentration is conducive to forming small-diameter fibers. As the concentration increases, beads show, and the fibers also appear to grow in size, as evidenced by the diameters observed in samples D (330 nm), E (349 nm), and F (0,52 µm), with 10%, 15%, and 20% polymer respectively. Remarkably, these electrospinning solutions also contained a non-electrospinnable silica solution despite its non-reactive nature to the electrospinning process.

Here, the decisive influence of polymer concentration in the overall process is highlighted, as it enabled the formation of fibers from blends that would not otherwise have been electrospun. Overall, these results demonstrate that the subtle combination of factors, such as polymer concentration and the inclusion of non-electrospinnable materials, can lead to surprising fiber formation results and offer new perspectives for the engineering of functional materials.

Comparing these results with the study carried out by Ren et al. [35] on silica nanofibers by centrifugal jet spinning, they observed that the presence and amount of PVP modified the properties of the spinning solution and that the average diameter of the fibers increased with increasing PVP content in the spinning solution.

Therefore, our study identified Sample C, which contains an 8% PVA solution, as the most advantageous fibrous structure among the tested specimens. It also exhibits fine fibers measuring 119 nm in diameter. This sample was also used to compare the effects of CPTS and TEOS. As observed in Fig. 2, the nanofibers with TEOS do not form a robust film. However, they are easily disintegrated, which is confirmed by SEM images indicating the presence of non-continuous fibers. The issues with the structural integrity observed in TEOS-based films arise from its natural tendency for rapid hydrolysis and condensation, resulting in the creation of three-dimensional silica networks [36, 37]. These networks are typically spatially unstructured, making the films prone to brittleness and fragmentation.

Conversely, CPTS features a chloropropyl functional group that enhances its compatibility with the polymer matrix, leading to more regulated and consistent hydrolysis and condensation processes [38]. This results in more uniform and cohesive films, significantly improving their structural integrity compared to those produced with TEOS. It leads to the forming a more stable and continuous silica network within the fibers, as evident in the cohesive films shown in Fig. 3c. The chloropropyl groups in CPTS may

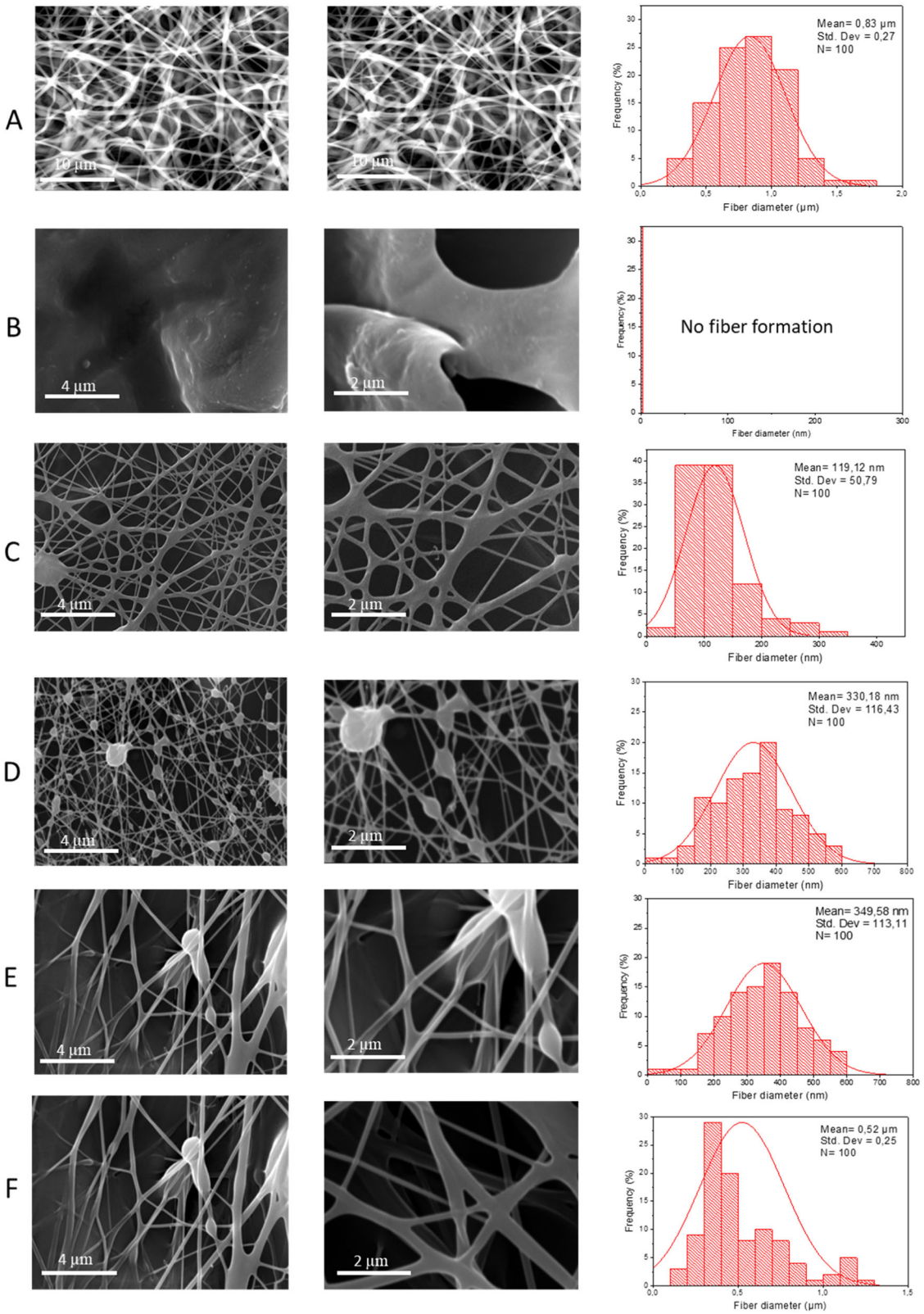

Fig. 1 SEM results and diameter distribution of hybrid nanofiber (Sample **A**, **B**, **C**, **D**, **E**, and **F**)

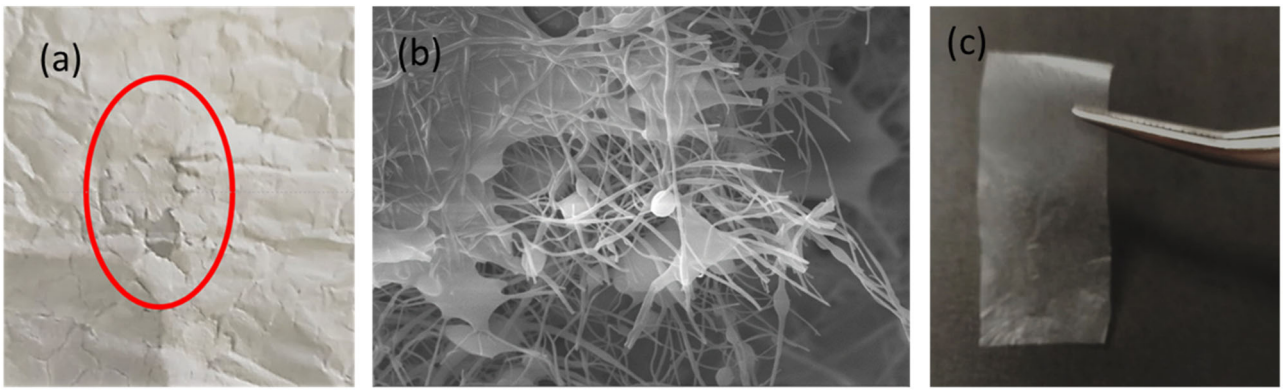

Fig. 2 **a** Image of electrospun hybrid nanofibers with TEOS (Sample T) **b** SEM results electrospun hybrid nanofibers with TEOS (Sample T) **c** Image of electrospun hybrid nanofibers with CPTS (Sample C)

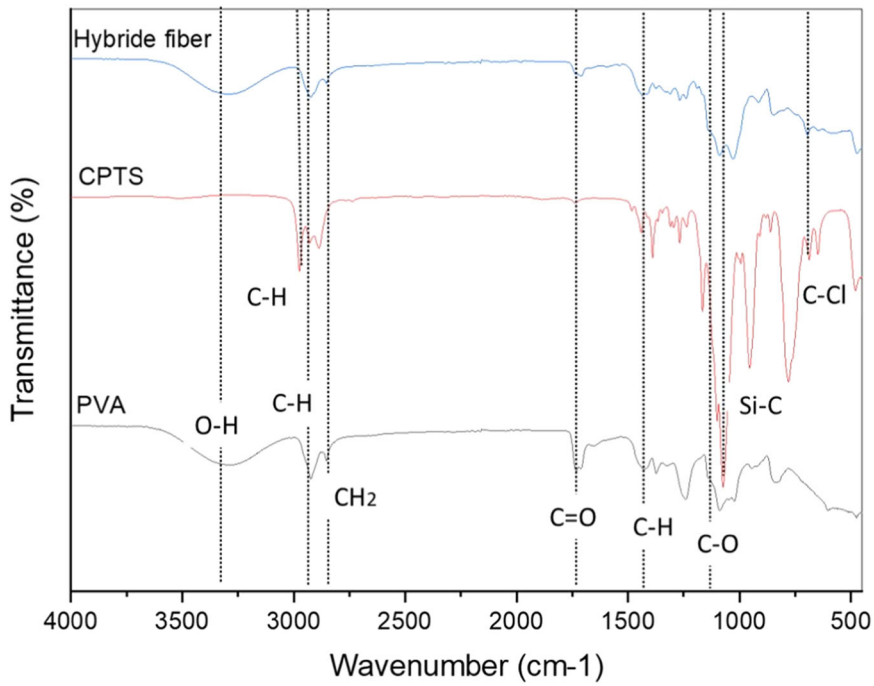

Fig. 3 FITR spectra of (**a**) PVA, CPTS, and hybrid nanofiber C

also engage in additional bonding interactions with the PVA, enhancing the films' mechanical strength and structural integrity.

3.2 Chemical Composition of Hybrid Nanofibers

FTIR was performed to study the chemical composition of hybrid nanofibers. Figure 3 shows the FTIR of the produced fibers. For the PVA nanofibers spectra, prominent characteristic peaks were observed at 3303 cm^{-1}, corresponding to O-H stretching vibrations indicative of hydrogen bonding [39]. Additionally, 2922 cm-1 and 2878 cm-1 peaks were attributed to C-H asymmetric stretching and CH2 symmetric stretching vibrations, respectively [40]. Peaks at 1428 cm^{-1} and 1088 cm^{-1} were associated with C-H symmetric stretching and C-O stretching vibrations, respectively [41]. In the CPTS spectra, notable peaks were observed at 2974 cm^{-1}, 2927 cm^{-1}, and 2886 cm^{-1}, attributed to C-H stretching vibrations. Additionally, peaks at 687 cm^{-1}, 780 cm^{-1}, and 1073 cm^{-1} indicated C–Cl, C-Si, and Si-O stretching vibration, respectively [42].

For the hybrid fiber spectra, the peak at 3296 cm^{-1} indicates the presence of O-H bonds, typical of PVA, suggesting the persistence of PVA functional groups in their composition. The peak at 2938 cm^{-1} is associated with C-H stretching vibrations, indicating the presence of alkyl

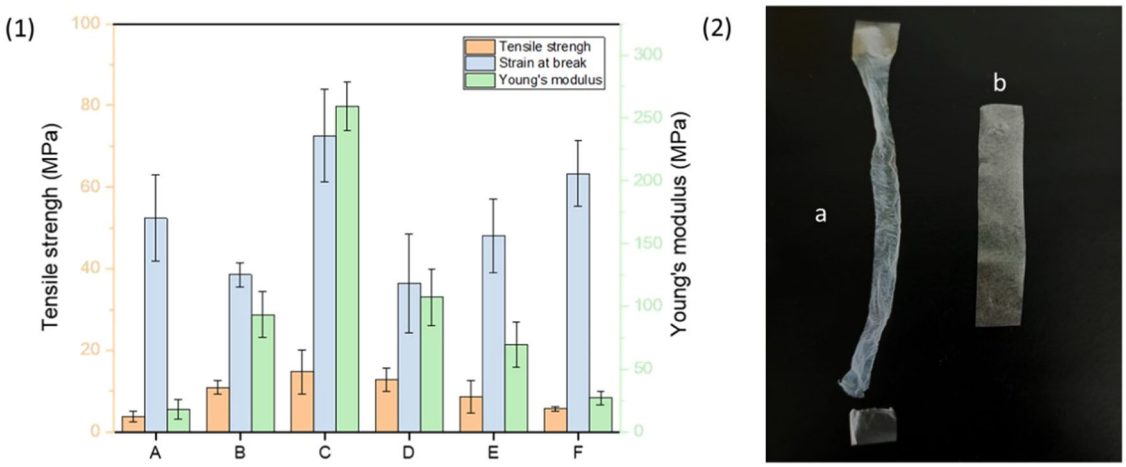

Fig. 4 (1) Tensile test results of hybrid nanofiber fiber; (2) specimen before **b** and after **a** tensile test (3)

groups from CPTS. The peak at 1734 cm^{-1} can be attributed to the stretching vibration of the C = O bond, suggesting the presence of acetyl or carbonyl groups in the composition. The peaks at 1428 cm-1 and 1088 cm-1were associated with C-H symmetric stretching and C-O stretching vibrations, moreover peaks at 1340 cm^{-1}, 1270 cm^{-1}, 1300 cm^{-1}, and 1239 cm^{-1} likely result from C-H and C-O vibrations specific to the PVA and CPTS possibly indicating interactions or bonding between the two components. Specifically, the peak at 697 cm^{-1} and 1073 cm^{-1} could be attributed to the C-Cl and C-Si vibration, respectively [43], indicating the presence of the characteristic silane bond of CPTS.

In summary, analysis of FTIR spectra of the hybrid nanofibers reveals the presence of functional groups and chemical bonds specific to PVA and CPTS, suggesting an interaction or bond between these two components. These results are in line with a similar study by Bramanti et al. [44], where FTIR spectroscopic analysis of electrospun tetraethylorthosilicate (TEOS) and Polyvinylpyrrolidone (PVP) microfibres showed that the TEOS silica precursor interacts with PVP, and the electrospinning process probably favors the formation of silica particles enveloped by PVP molecules.

3.3 Tensile Test

Tensile test results of hybrid fibers (Fig. 4 and Table 2) in response to variations in the percentage of polymer in solution reveal the resulting fibers' distinct and informative mechanical characteristics. The tensile strength of control sample A represents reference conditions with 8% of PVA, values of 3.8 MPa, Young's modulus of 18 MPa, and a strain at break of 52%. In contrast, sample B shows an apparent increase in tensile strength, reaching 10.9 MPa and a substantial Young's modulus of 93.4 MPa. However, this enhancement in strength is accompanied by a noticeable reduction in elongation at break, which decreases to 38.5%. The increase in tensile strength and Young's modulus in Sample B can be attributed to a higher degree of polymer chain alignment, resulting in a stiffer and stronger fiber, while the reduction in elongation at break suggests a trade-off between strength and flexibility.

Table 2 Tensile test results of hybrid nanofiber

Sample	Tensile strength (MPa)	Young's modulus (MPa)	Strain at break (%)
A	3.8 ± 1.3	18.2 ± 7.8	52.4 ± 10.6
B	10.9 ± 1.6	93.4 ± 18.3	38.5 ± 3.0
C	14.7 ± 5.5	259.3 ± 19.0	72.6 ± 11.4
D	12.8 ± 2.8	107.2 ± 22.8	36.4 ± 12.2
E	8.6 ± 4.0	69.6 ± 17.6	48.1 ± 9.0
F	5.7 ± 0.5	27.2 ± 5.4	63.3 ± 8.0

Similarly, for sample C, we observe a continuous increase in tensile strength, which reaches 14.7 MPa, along with a remarkable Young's modulus of 259 MPa. Importantly, this sample maintains a high elongation at a break of 72.6%. This suggests an optimal balance between crystallinity and polymer chain mobility at this specific concentration of 8% PVA, enhancing stiffness and flexibility.

Samples D, E, and F exhibit marked variations in their mechanical characteristics. In particular, samples D and E show tensile strengths of 12,8 MPa and 8,6 MPa, Young's modulus of 107 MPA and 69,6 MPa, and an elongation at break of 36,4% and 348,1%, respectively. Sample F stands out due to its comparable elongation at break (63.3%) despite a reduction in tensile strength to 4.46 MPa and a Young's modulus of 27.2 MPa. The differences in

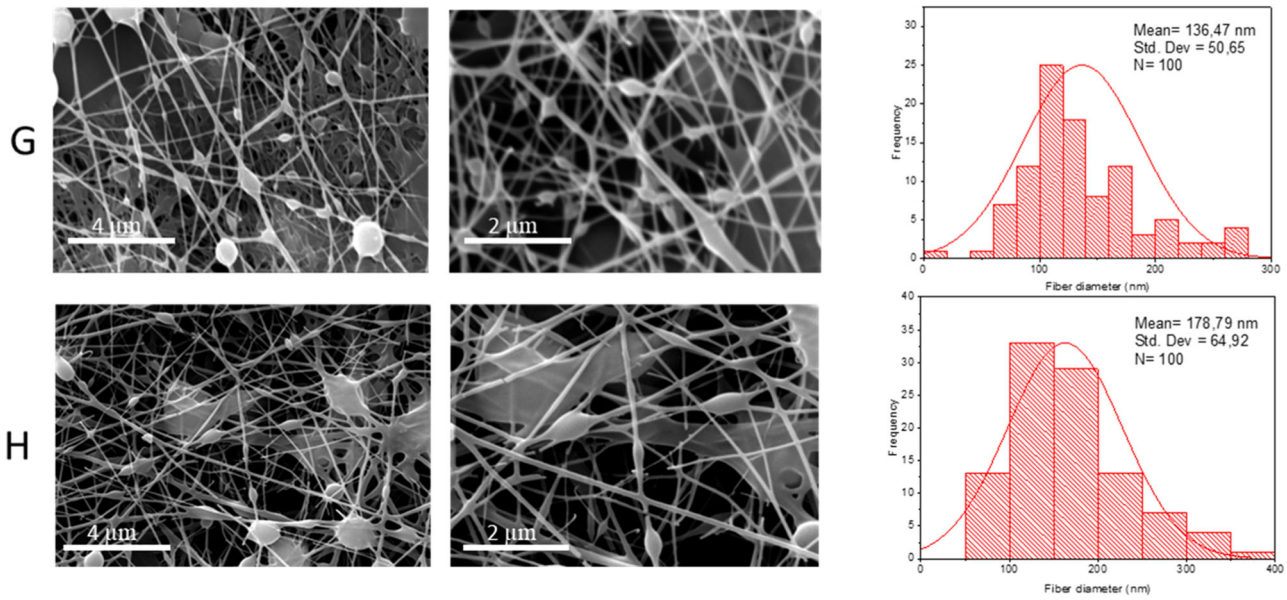

Fig. 5 SEM results of antibacterial hybrid fiber (Sample G and F)

mechanical properties among these samples can be linked to variations in fiber diameter, with smaller diameters generally leading to higher tensile strength and modulus due to a more compact and uniform fiber structure.

These findings highlight the relationship between polymer concentration and fiber mechanical properties. In particular, Sample C (8% PVA solution in the composition) stands out as the most favorable option among the tested specimens because it combines both a high Young's modulus (259 MPa) and an impressive strain at break (72.6%). This means that the material in sample C is relatively stiff and can maintain its structural integrity under load while stretching significantly before breaking. Such a combination is valuable in various engineering and industrial applications requiring strength and flexibility. It offers the best compromise between these essential mechanical properties, making it a versatile choice for various applications.

3.4 BAC-Doped Hybrid Nanofibers

Sample C, incorporating an 8% PVA solution, was chosen for developing the hybrid nanofiber due to its superior mechanical properties and advantageous fibrous structure. These attributes make Sample C the most favorable option among the tested specimens and an ideal candidate for incorporating BAC to achieve enhanced antibacterial activity

3.4.1 Morphologies of Hybrid Nanofiber

The results from SEM (Fig. 5), with the addition of BAC, have unveiled some intriguing patterns in the formation of electrospun fibers, with certain beads indicating the encapsulation of this agent. In samples G and H, the electrospun fibers exhibited diameters of 136.5 nm and 178.8 nm, respectively. These measurements establish a reference point for the typical size of the fibers under the influence of BAC. These findings suggest that the presence of BAC during the electrospinning process can influence the fiber morphology, possibly leading to the formation of beads and affecting the final fiber size.

3.4.2 Element Composition

Figure 6 presents the EDX analysis spectra of fibers. Sample C spectra reveal that the nanofibers predominantly comprise PVA with approximately 67.86% carbon, 27.66% oxygen, 3.44% silicon, and 1.04% chlorine by weight. These elements confirm the hybrid structure composed of PVA and silica-related components [45, 46] —adding BAC in Samples G and H results in noticeable changes in their elemental composition. Specifically, introducing BAC increases the nitrogen content to 4.77 and 5.19% by weight for Samples G and H, respectively, and leads to variations in the proportions of oxygen, silicon, and chlorine. For example, Sample G contains 3.34% chlorine, while Sample H contains 2.69% chlorine by weight. These changes suggest that BAC integrates into the nanofiber matrix, potentially altering the polymer chain alignment and crystallinity. The presence of nitrogen and chlorine, introduced by BAC, indicates the successful incorporation of the antibacterial agent, while the slight shifts in other elemental concentrations reflect the modification of the nanofiber's chemical environment. This characterization provides valuable insights into the

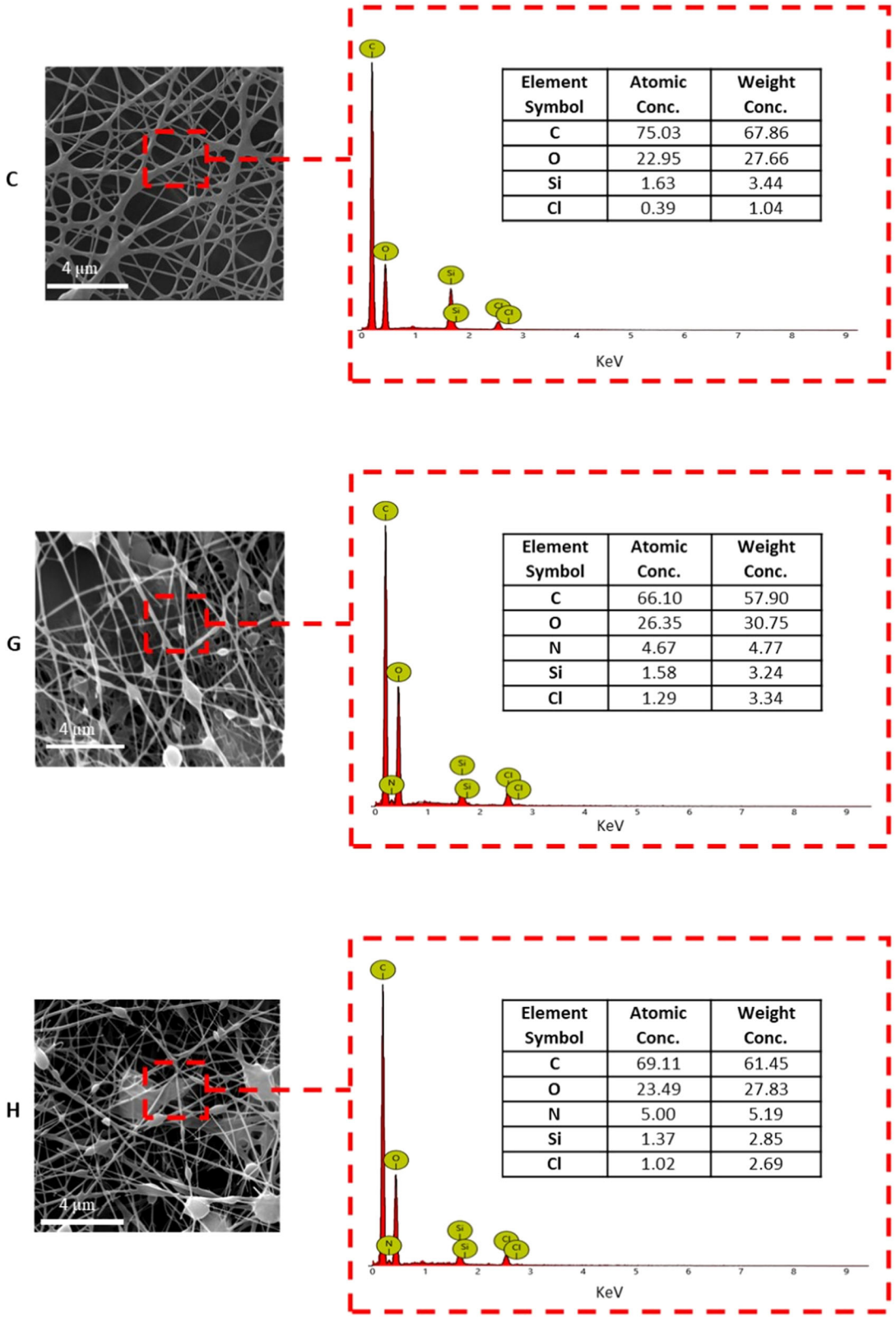

Fig. 6 EDX spectra of the antibacterial hybrid nanofiber (Sample C, G, and H)

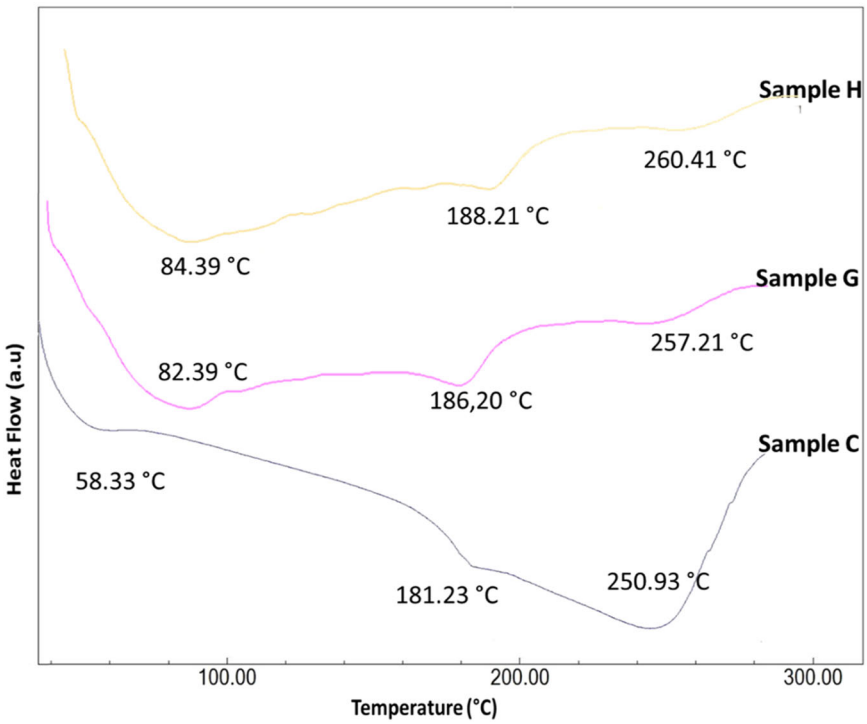

Fig. 7 DSC analysis curve of the antibacterial hybrid nanofiber (Sample C, G, and H)

material's composition and aids in further understanding and optimizing its properties for specific applications, particularly in enhancing antibacterial activity.

3.4.3 Thermal Stability

From SEM results shown in Fig. 7, sample C. exhibited three distinct temperature points: 58 °C, 181 °C, and 250 °C. The initial temperature of 58 °C likely signifies a low-temperature transition or event, potentially associated with the hygroscopic nature of PVA, where absorbed moisture may influence this thermal transition. Alternatively, this temperature could be close to the glass transition temperature (Tg) of PVA, depending on its water content, possibly associated with a modification in the amorphous structure of the hybrid nanofiber. The second temperature, observed at 181 °C, is notably close to the literature-reported melting temperature of PVA, which typically falls within the 160–180 °C [47]. This alignment implies the sustained presence of the PVA phase within the hybrid fiber, corroborating the findings from the FTIR analysis that indicated the persistence of PVA functional groups in the composition. The proximity of this temperature to the known melting point of PVA strengthens the argument for the successful integration of PVA into the hybrid structure.

The third temperature point, at 250 °C, suggests a higher-temperature transition or thermal decomposition. This temperature range points to another component in the hybrid fiber with a distinct thermal response, possibly associated with the CPTS. This finding emphasizes the nature of the hybrid fiber composition, characterized by multiple thermal transitions corresponding to different components within its structure. Notably, the inclusion of silica in the hybrid structure is known to impart thermal stability [48]. Thus, the observed higher-temperature transition at 250 °C may be attributed to the reinforcing effect of silica. This suggests that the silica component contributes to elevating the overall thermal resistance of the hybrid fiber, a crucial aspect for potential applications in elevated-temperature environments.

The results are consistent with a similar study on the fabrication s of polyacrylonitrile-silica fibers using electrospinning [49]. The addition of tetraethyl orthosilicate (TEOS) to polyacrylonitrile (PAN) in producing carbon-silica hybrid nanofibers has been shown to enhance their thermal properties. The incorporation of TEOS contributes to improving thermal stability and other characteristics.

The DSC analysis reveals additional insights for the incorporated Samples G and H with BAC. Sample G shows thermal transitions at 82.39 °C, 186.20 °C, and 257.21 °C, while Sample H exhibits transitions at 84.39 °C, 188.21 °C, and 260.41 °C. The initial transitions for both samples are higher than Sample C, indicating that BAC influences the thermal behavior of the hybrid nanofibers, possibly due to its integration into the polymer matrix, which can alter the molecular interactions and thermal stability. The second transitions are slightly elevated compared to Sample C, suggesting that BAC's presence modifies the melting behavior of the PVA phase. The higher third temperature

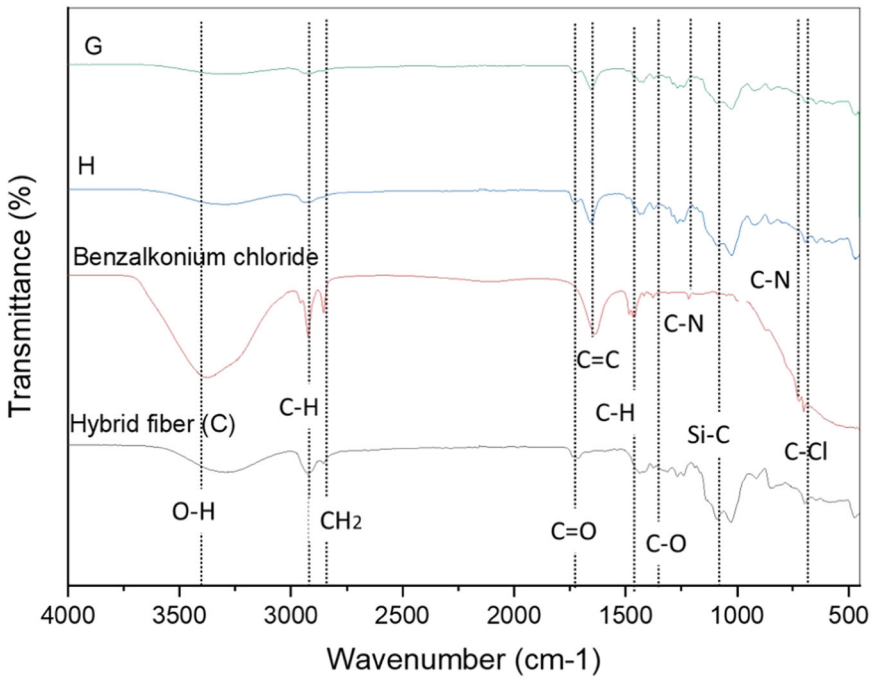

Fig. 8 FITR spectra of Benzalkonium chloride and antibacterial hybrid nanofiber C, G, and H

points indicate that BAC contributes to increased thermal resistance, further supporting the idea that integrating BAC enhances the overall thermal stability of the hybrid fibers. The enhancement of thermal properties by BAC can be attributed to its interaction with the polymer matrix. Literature suggests that ammonium compounds like BAC can form strong ionic interactions with the polymer chains, leading to a more stabilized structure and higher thermal resistance [50]. The presence of BAC may also contribute to forming a more crosslinked network within the nanofiber structure, further enhancing thermal stability.

In summary, the DSC analysis of the PVA-Silica hybrid nanofiber unravels a multifaceted thermal profile. The identified temperatures suggest distinct thermal events related to different components of the hybrid fiber, providing crucial insights into its thermal behavior and highlighting the successful integration of PVA with CPTS. The addition of BAC further enhances the thermal properties, making the hybrid nanofibers suitable for a broader range of applications requiring antibacterial activity and high thermal stability.

3.4.4 Chemical Composition

The chemical structure of BAC must first be examined for the antibacterial hybrid nanofiber. The FTIR spectra of BAC (Fig. 8) provide detailed insights into its chemical composition and structure. Several characteristic absorbance peaks were observed in the infrared spectrum. The peak at 3373 cm^{-1} corresponds to the stretching vibration of the O-H stretching vibrations. The peaks at 2923 cm^{-1} and 2853 cm^{-1} are associated with asymmetric and symmetric C-H stretching vibrations, respectively, revealing the presence of alkyl groups in the compound. At 1654 cm^{-1}, a peak may suggest a C = C vibration, potentially arising from the benzene-like groups in the structure of BAC. The peaks at 1467 cm^{-1} and 1377 cm^{-1} are attributable to C-H deformation vibrations, while those at 1216 cm^{-1} may correspond to C-N deformation vibrations in the quaternary ammonium moiety. The 722 cm^{-1} and 701 cm-1 peaks could be related to C-Cl and C-N deformation vibrations, respectively [42], further confirming the presence of characteristic functional groups in this compound. These results reflect a detailed analysis of the molecular vibrations of pure BAC.

For the infrared spectra of samples G and H, containing 0.1 and 1% BAC, respectively, the peaks are similar to those of sample C, except for the appearance of a new peak at 1654 cm^{-1}. This peak is associated with the C = C vibration, a BAC characteristic. This observation suggests that BAC integrates significantly into the chemical composition of the hybrid fibers, indicating an effective interaction between the antibacterial agent and the hybrid material.

3.4.5 Tensile Test

The mechanical properties of antibacterial hybrid nanofibers incorporating BAC, as shown in Fig. 9 and Table 3, reveal distinct characteristics. Samples G and H exhibit slightly lower tensile strengths of 13.1 MPa and 12.4 MPa, Young's moduli of 230 MPa and 220 MPa, and less impressive elongations at break of 63% and 53.2%, respectively. The incorporation of BAC slightly reduces the mechanical

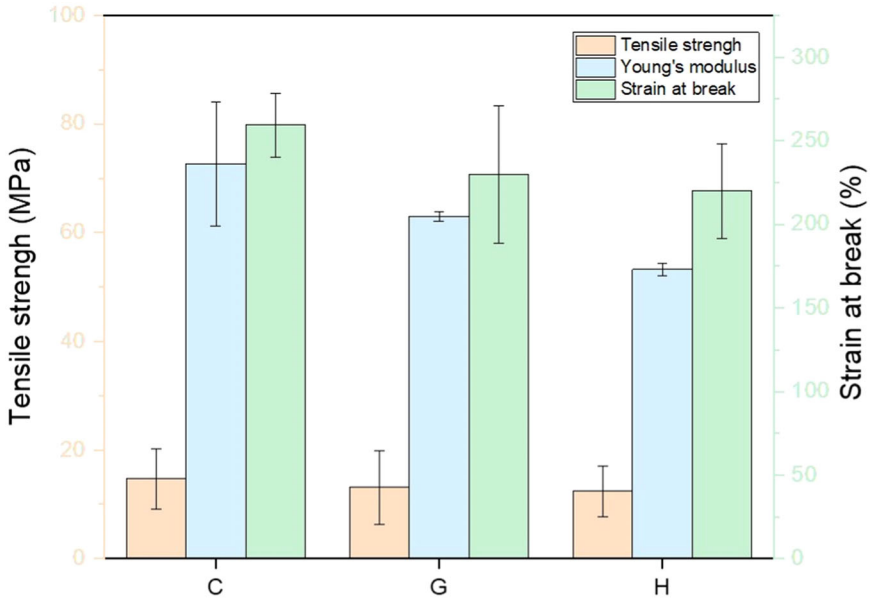

Fig. 9 Tensile test results of antibacterial hybrid nanofiber (C, G, and H)

Table 3 Tensile test results of antibacterial hybrid nanofiber

Sample	Tensile strength (MPa)	Young's modulus (MPa)	Strain at break (%)
C	**14.7 ± 5.5**	**259.3 ± 19.0**	**72.6 ± 11.4**
G	**13.1 ± 6.7**	**230.0 ± 41.2**	**63.0 ± 0.9**
H	**12.4 ± 4.6**	**220.0 ± 28.2**	**53.2 ± 1.2**

properties compared to Sample C. This decrease can be attributed to the interaction between BAC and the polymer matrix. BAC may disrupt the uniform polymer chain alignment and crystalline structure, reducing tensile strength and Young's modulus. Additionally, the presence of BAC could introduce microvoids or defects within the fiber structure, contributing to decreased mechanical properties.

Despite this, the decrease is minor. Samples G and H maintain strong tensile strength and Young's modulus values, indicating they remain mechanically robust. This suggests that the addition of BAC has only a minimal impact on the overall mechanical properties of the material. The fibers retain their strength and functionality for many applications while offering the added benefit of antibacterial properties.

3.4.6 Antibacterial Activity

The antibacterial activities of hybrid nanofiber against Gram-positive S. aureus and Gram-negative E. coli were evaluated by disc inhibition zone method. The ability of the hybrid nanofiber to inhibit the growth of the tested microorganisms is shown in Fig. 10. Observation of bacterial growth inhibition diameters for samples G and H (at 0.1 and 1% antibacterial agent, respectively) reveals a significant variation in antimicrobial efficacy. Sample H, with a higher concentration of 1% antibacterial agent, generated a larger zone of bacterial growth inhibition (20 mm) than sample G (12 mm) with 0.1% antibacterial agent. This difference in diameter suggests that sample H has a higher capacity to inhibit bacterial growth, indicating more robust antimicrobial activity. Similarly, for E. coli, Sample H, with a higher concentration of 1% BAC, produced a larger zone of bacterial growth inhibition (9.2 mm) compared to Sample G (7.1 mm) with 0.1% BAC. This result supports the conclusion that higher concentrations of BAC result in more effective inhibition of bacterial growth.

The enhanced antimicrobial activity can be attributed to the mechanism by which BAC kills bacteria. BAC disrupts bacterial cell membranes by integrating its hydrophobic tail into the membrane, causing lipid diffusion and membrane destabilization. Then, it leads to leakage of intracellular contents, degradation of nucleic acids and proteins, and, ultimately, cell death [51]. BAC also interferes with bacterial metabolism and can penetrate the cell membrane, enhancing its lethal effect [32]. Consequently, adding 1% BAC appears to have a more pronounced impact on inhibiting Staphylococcus and E. coli bacteria than the lower concentration of 0.1%.

4 Conclusion

Overall, these results highlight the complexity of hybrid fibers and how subtle combinations of factors, such as polymer concentration and the inclusion of non-electrospinnable

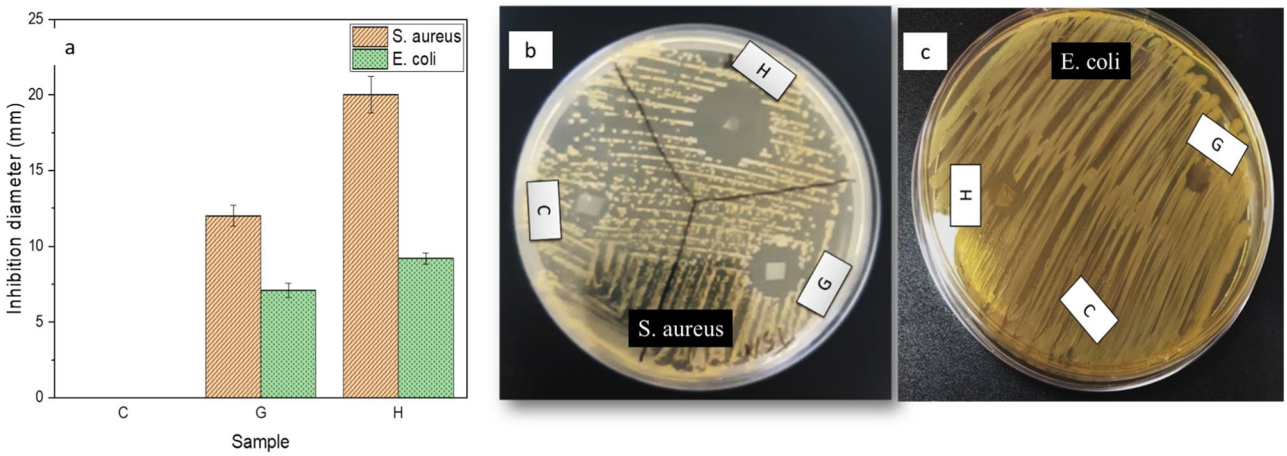

Fig. 10 Antibacterial activity results: **a** bacterial growth inhibition diameters **b** inhibition against S.aureus **c** inhibition against E.coli

materials, can influence their formation and properties. Sample C, combined with an 8% PVA solution, stands out as the best option in terms of fibrous structure, with fine fibers measuring 119 nm in diameter and excellent mechanical properties, including a high Young's modulus and impressive tensile strength. Chemical composition analysis through infrared and EDX confirmed the presence of silica-related components in the hybrid structure. Additionally, adding BAC demonstrated the ability to inhibit bacterial growth in the hybrid fibers. Sample H, containing 1% BAC, showed significant bacterial growth inhibition (20 mm for *S. aureus* and 9.2 mm for *E. coli*), along with enhanced thermal stability (260.41 °C) and tensile strength (12.4 MPa). These findings suggest that these antibacterial nanofibers have potential applications in various medical fields, such as surgical gowns, wound dressings, hospital linens, face masks, and gloves. These results pave the way for new perspectives in developing hybrid nanofibers via electrospinning, particularly for advanced medical applications.

Data Availability

No datasets were generated or analysed during the current study.

Acknowledgements This research was supported by the National Center for Scientific and Technical Research (CNRST) of Morocco (grant number 13UH22020). We extend our heartfelt thanks to Mohammed VI Polytechnic University in Morocco, and the Center for Nanotechnology & Biomaterials Applications and Research (NBUAM) at Marmara University in Turkey, for their generous support in conducting some analytical tests in their laboratories. Your support significantly enriched the quality of our research.

Author contributions •Khadija EL KALAAOUI: Conceptualization, Data curation, Formal analysis, Writing – original draft •aicha BOUKHRISS: Investigation, Methodology, Validation, Writing – review & editing •Oumaima BILI: Data curation, Formal analysis, Writing – original draft •Mohamed AIT CHAOUI R0: Investigation, Methodology, •sanaa Majid: Methodology, Validation, Writing – review & editing •Mohamed EL HAJAJI: Visualization, Writing – review & editing •said GMOUH : Methodology, Project administration, Supervision, Validation, Writing – review & editing.

Compliance with ethical standards

Conflict of interest The authors declare no competing interests.

References

1. Abadi B, Goshtasbi N, Bolourian S, Tahsili J, Adeli-Sardou M, Forootanfar H (2022) Electrospun hybrid nanofibers: fabrication, characterization, and biomedical applications. Front Bioeng Biotechnol 10:986975. https://doi.org/10.3389/fbioe.2022.986975.
2. Kanjwal MA, Ghaferi AA (2022) Hybrid nanofibers opportunities and frontiers – a review. J Environ Chem Eng 10(6):108850. https://doi.org/10.1016/j.jece.2022.108850.
3. SM Sadeghi (2021) 3D networks of TiO2 nanofibers fabricated by sol-gel/electrospinning/calcination combined method: valuation of morphology and surface roughness parameters. *Mater Sci.* 271, 115254. https://doi.org/10.1016/j.mseb.2021.115254
4. Chen S, Zhou J, Fang B, Ying Y, Yu D, He H (2024) Three EHDA processes from a detachable spinneret for fabricating drug fast dissolution composites. Macro Mater Eng 309(4):2300361. https://doi.org/10.1002/mame.202300361.
5. Gong W, Yang W, Zhou J, Zhang S, Yu DG, Liu P (2024) Engineered beads-on-a-string nanocomposites for an improved drug fast-sustained bi-stage release. Nanocomposites 10(1):240–253. https://doi.org/10.1080/20550324.2024.2362477.
6. Huang C, Wang M, Yu S, Yu DG, Bligh SWA (2024) Electrospun fenoprofen/polycaprolactone @ tranexamic acid/hydroxyapatite nanofibers as orthopedic hemostasis dressings. Nanomaterials 14(7):646. https://doi.org/10.3390/nano14070646.
7. Zhou J, Pan H, Gong W, Yu DG, Sun Y (2024) Electrosprayed Eudragit RL100 nanoparticles with Janus polyvinylpyrrolidone patches for multiphase release of paracetamol. Nanoscale 16(17):8573–8582. https://doi.org/10.1039/D4NR00893F
8. Wang M, Hou J, Yu DG, Li S, Zhu J, Chen Z (2020) Electrospun tri-layer nanodepots for sustained release of acyclovir. J Alloy Compd 846:156471. https://doi.org/10.1016/j.jallcom.2020.156471.

9. Xu L et al. (2024) Electrospun multi-functional medicated trisection Janus nanofibers for an improved anti-adhesion tendon repair. Chem Eng J 492:152359. https://doi.org/10.1016/j.cej.2024.152359.
10. Zhao P et al. (2024) Electrospun trilayer eccentric Janus nanofibers for a combined treatment of periodontitis. Adv Fiber Mater 6(4):1053–1073. https://doi.org/10.1007/s42765-024-00397-6.
11. Yu D, Gong W, Zhou J, Liu Y, Zhu Y, Lu X (2024) Engineered shapes using electrohydrodynamic atomization for an improved drug delivery. WIREs Nanomed Nanobiotechnol 16(3):e1964. https://doi.org/10.1002/wnan.1964.
12. Sun Y, Zhou J, Zhang Z, Yu DG, Bligh SWA (2024) Integrated Janus nanofibers enabled by a co-shell solvent for enhancing icariin delivery efficiency. Int J Pharm 658:124180. https://doi.org/10.1016/j.ijpharm.2024.124180
13. Alam MR, Shahid MA, Alimuzzaman S, Hasan MM, Hoque ME (2023) Electrospun bio-nano hybrid scaffold from collagen, *Nigella sativa*, and chitosan for skin tissue engineering application. J Bioact Compat Polym 38(3):234–251. https://doi.org/10.1177/08839115231162365.
14. Hasan MM, Shahid MA (2023) PVA, licorice, and collagen (PLC) based hybrid bio-nano scaffold for wound healing application. J Biomater Sci Polym Ed 34(9):1217–1236. https://doi.org/10.1080/09205063.2022.2163454.
15. Shahid MdA, Hasan MdM, Alam MR, Mohebullah M, Chowdhury MA (2022) Antibacterial multicomponent electrospun nanofibrous mat through the synergistic effect of biopolymers. J Appl Biomater Funct Mater 20:228080002211360. https://doi.org/10.1177/22808000221136061.
16. Shahid MdA et al. (2021) Antibacterial wound dressing electrospun nanofibrous material from polyvinyl alcohol, honey *and Curcumin longa* extract. J Ind Text 51(3):455–469. https://doi.org/10.1177/1528083720904379.
17. Li L et al. (2023) Electrospinning technology on one dimensional microwave absorbers: fundamentals, current progress, and perspectives. Chem Eng J 470:144236. https://doi.org/10.1016/j.cej.2023.144236.
18. Matsuura T, Shirazi MMA (2023) Principles of electrospinning and nanofiber membranes. in *Electrospun and Nanofibrous Membranes*, Elsevier, p. 3–25. https://doi.org/10.1016/B978-0-12-823032-9.00016-7.
19. Liu Y et al. (2023) Scale-up strategies for electrospun nanofiber production. in *Electrospun and Nanofibrous Membranes*, Elsevier, p. 205–266. https://doi.org/10.1016/B978-0-12-823032-9.00020-9.
20. Li SF, Hu TG, Wu H (2023) Fabrication of colon-targeted ethyl cellulose/gelatin hybrid nanofibers: regulation of quercetin release and its anticancer activity, *Int J Biol Macromol*, p. 127175. https://doi.org/10.1016/j.ijbiomac.2023.127175.
21. Zhang J, Li J, Zeng XF, Wang JX, Le Y (2023) Double-layer hybrid nanofiber membranes by electrospinning with sustained antibacterial activity for wound healing. J Ind Eng Chem 127:416–425. https://doi.org/10.1016/j.jiec.2023.07.025.
22. Pepe Y, Akkoyun S, Bozkurt B, Karatay A, Ates A, Elmali A (2023) Investigation of the wavelength dependent nonlinear absorption mechanisms of polyvinylpyrrolidone and cadmium selenide hybrid nanofibers. Opt Laser Technol 164:109497. https://doi.org/10.1016/j.optlastec.2023.109497.
23. Aher PD, Patil YD, Waysal SM, Bhoi AM (2023) Critical review on biopolymer composites used in concrete. Mater Today Proc, p. S2214785323040828. https://doi.org/10.1016/j.matpr.2023.07.212.
24. Platnieks O, Beluns S, Briede S, Jurinovs M, Gaidukovs S (2023) Cellulose synergetic interactions with biopolymers: Functionalization for sustainable and green material design. Ind Crops Prod 204:117310. https://doi.org/10.1016/j.indcrop.2023.117310.
25. Li L et al. (2021) Research progress of ultrafine alumina fiber prepared by sol-gel method: a review. Chem Eng J 421:127744. https://doi.org/10.1016/j.cej.2020.127744.
26. Innocenzi P (2023) Sol-gel processing for advanced ceramics, a perspective, *Open Ceramics*, p. 100477, https://doi.org/10.1016/j.oceram.2023.100477.
27. Malucelli G (2020) Sol–gel technique for protective textile and clothing, in *Advances in Functional and Protective Textiles*, Elsevier, p. 1–17. https://doi.org/10.1016/B978-0-12-820257-9.00001-1.
28. Mathew Simon S et al. (2021) Recent advancements in multifunctional applications of sol-gel derived polymer incorporated TiO2-ZrO2 composite coatings: a comprehensive review. Appl Surf Sci Adv 6:100173. https://doi.org/10.1016/j.apsadv.2021.100173.
29. Yanilmaz M, Lu Y, Zhu J, Zhang X (2016) Silica/polyacrylonitrile hybrid nanofiber membrane separators via sol-gel and electrospinning techniques for lithium-ion batteries. J Power Sources 313:205–212. https://doi.org/10.1016/j.jpowsour.2016.02.089.
30. Jafari MT, Saraji M, Kermani M (2018) Sol-gel electrospinning preparation of hybrid carbon silica nanofibers for extracting organophosphorus pesticides prior to analyzing them by gas chromatography-ion mobility spectrometry. J Chromatogr A 1558:1–13. https://doi.org/10.1016/j.chroma.2018.05.014.
31. Mohamady Hussein MA et al. (2021) Chitosan/gold hybrid nanoparticles enriched electrospun PVA nanofibrous mats for the topical delivery of Punica Granatum l. extract: synthesis, characterization, biocompatibility and antibacterial properties. IJN 16:5133–5151. https://doi.org/10.2147/IJN.S306526.
32. Larsson Y, Mongelli A, Kisielius V, Bester K (2024) Microbial biofilm metabolization of benzalkonium compounds (benzyl dimethyl dodecyl ammonium & benzyl dimethyl tetradecyl ammonium chloride). J Hazard Mater 463:132834. https://doi.org/10.1016/j.jhazmat.2023.132834.
33. Forbes S, Morgan N, Humphreys GJ, Amézquita A, Mistry H, McBain AJ (2019) Loss of function in escherichia coli exposed to environmentally relevant concentrations of benzalkonium chloride. Appl Environ Microbiol 85(4):e02417–e02418. https://doi.org/10.1128/AEM.02417-18.
34. Khoerunnisa F et al. (2021) Toughened chitosan-based composite membranes with antibiofouling and antibacterial properties *via* incorporation of benzalkonium chloride. RSC Adv 11(27):16814–16822. https://doi.org/10.1039/D1RA01830B
35. Ren L, Ozisik R, Kotha SP (2014) Rapid and efficient fabrication of multilevel structured silica micro-/nanofibers by centrifugal jet spinning. J Colloid Interface Sci 425:136–142. https://doi.org/10.1016/j.jcis.2014.03.039.
36. Malay O, Yilgor I, Menceloglu YZ (2013) Effects of solvent on TEOS hydrolysis kinetics and silica particle size under basic conditions. J Sol Gel Sci Technol 672):351–361. https://doi.org/10.1007/s10971-013-3088-4.
37. Chou KT, Lee BI (1993) Properties of silica gels prepared from high-acid hydrolysis of tetraethoxysilane. Ceram Int 19(5):315–325. https://doi.org/10.1016/0272-8842(93)90044-R.
38. Moretto E et al. (2022) Dual-silane premodified silica nanoparticles—synthesis and interplay between chemical, mechanical, and curing properties of silica–rubber nanocomposites: application to tire tread compounds. ACS Omega 7(21):17692–17702. https://doi.org/10.1021/acsomega.2c00665.
39. Blout ER, Karplus R (1948) The infrared spectrum of polyvinyl alcohol. J Am Chem Soc 70(2):862–864. https://doi.org/10.1021/ja01182a504.
40. Mansur HS, Sadahira CM, Souza AN, Mansur AAP (2008) FTIR spectroscopy characterization of poly (vinyl alcohol) hydrogel with different hydrolysis degree and chemically crosslinked with

glutaraldehyde. Mater Sci Eng C 28(4):539–548. https://doi.org/10.1016/j.msec.2007.10.088.
41. Hussein MAM, Gunduz O, Sahin A, Grinholc M, El-Sherbiny IM, Megahed M (2022) Dual spinneret electrospun polyurethane/PVA-gelatin nanofibrous scaffolds containing cinnamon essential oil and nanoceria for chronic diabetic wound healing: preparation, physicochemical characterization and in-vitro evaluation. Molecules 27(7):2146. https://doi.org/10.3390/molecules27072146.
42. Tepekiran BN, Calisir MD, Polat Y, Akgul Y, Kilic A (2019) Centrifugally spun silica (SiO_2) nanofibers for high-temperature air filtration. Aerosol Sci Technol 53(8):921–932. https://doi.org/10.1080/02786826.2019.1613514.
43. Vareda JP, Fonseca AC, Ribeiro ACF, Pontinha ADR (2024) Silica-Poly(Vinyl Alcohol) Composite aerogel: a promising electrolyte for solid-state sodium batteries. Gels 10(5):293. https://doi.org/10.3390/gels10050293.
44. Bramanti E, Bonaccorsi L, Campanella B, Ferrari C, Malara A, Freni A (2022) Structural characterization of electrospun tetraethylortosilicate (TEOS)/Polyvinylpyrrolidone (PVP) microfibres. Mater Chem Phys 287:126248. https://doi.org/10.1016/j.matchemphys.2022.126248.
45. Small-angle X-ray scattering and FTIR characterization of nanostructured poly (vinyl alcohol)/silicate hybrids for immunoassay applications | J Mater Sci. Consulté le: 2024. [En ligne]. Disponible sur: https://link.springer.com/article/10.1007/s10853-007-1953-7
46. Fahmy A, Mohamed TA, Abu-Saied M, Helaly H, El-Dossoki F (2020) Structure/property relationship of polyvinyl alcohol/dimethoxydimethylsilane composite membrane: experimental and theoretical studies. Spectrochim Acta Part A Mol Biomolecul Spectrosc 228:117810. https://doi.org/10.1016/j.saa.2019.117810.
47. Tsioptsias C, Fardis D, Ntampou X, Tsivintzelis I, Panayiotou C (2023) Thermal behavior of poly(vinyl alcohol) in the form of physically crosslinked film. Polym 15(8):1843. https://doi.org/10.3390/polym15081843.
48. Kim D, Chung I, Kim G (2013) Study on mechanical and thermal properties of fiber-reinforced Epoxy/Hybrid-silica composite. Fibers Polym 14(12):2141–2147. https://doi.org/10.1007/s12221-013-2141-9.
49. Pirzada T, Arvidson SA, Saquing CD, Shah SS, Khan SA (2014) Hybrid carbon silica nanofibers through Sol–Gel electrospinning. Langmuir 30(51):15504–15513. https://doi.org/10.1021/la503290n.
50. Zhang X et al. (2023) Benzalkonium chloride modified kaolinite with rapid bactericidal activity for the development of antibacterial films. Mater Today Commun 35:106152. https://doi.org/10.1016/j.mtcomm.2023.106152.
51. McCarlie SJ, Du Preez LL, Hernandez JC, Boucher CE, Bragg RR (2024) Transcriptomic signature of bacteria exposed to benzalkonium chloride. Res Microbiol 175(no 4):104151. https://doi.org/10.1016/j.resmic.2023.104151.